Electrochemistry Communications 115 (2020) 106740

Contents lists available at ScienceDirect

Electrochemistry Communications

journal homepage: www.elsevier.com/locate/elecom

In situ synchrotron X-ray diffraction study of the electrochemical reduction of SiO_2 in molten $CaCl_2$

Yumi Katasho[a,1], Yutaro Norikawa[a], Takayuki Yamamoto[a], Kouji Yasuda[b,c,2], Toshiyuki Nohira[a,*]

[a] Institute of Advanced Energy, Kyoto University, Gokasho, Uji, Kyoto 611-0011, Japan
[b] Agency for Health, Safety and Environment, Kyoto University, Yoshida-hommachi, Sakyo-ku, Kyoto 606-8501, Japan
[c] Department of Fundamental Energy Science, Graduate School of Energy Science, Kyoto University, Yoshida-hommachi, Sakyo-ku, Kyoto 606-8501, Japan

ARTICLE INFO

Keywords:
Molten salt
In situ analysis
Energy-dispersive X-ray diffraction
SiO_2
Electrochemical reduction
$CaCl_2$

ABSTRACT

In situ synchrotron X-ray diffraction was used to investigate the electrochemical reduction of SiO_2 to Si in molten $CaCl_2$ at 1123 K for the first time. The present technique enabled direct determination of intermediate products at high temperature, without cooling and washing treatments. Based on the diffraction data, the Ca_2SiO_4 phase was detected inside the electrode, but not at the electrode edge. These results were explained by the presence of different concentrations of O^{2-} ions in molten $CaCl_2$ permeating different regions of the electrode.

1. Introduction

Electrochemical reduction of SiO_2 in high-temperature molten salts has been attracting considerable attention as a new process for the production of high-purity silicon from SiO_2 [1–11]. This process has the potential to produce solar-grade silicon to replace the conventional (Siemens) process. Recently, electrochemical reduction of borosilicate glasses (whose main component is SiO_2) has also been investigated for application in a new recovery process of long-lived fission products from vitrified wastes [12–14].

The electrochemical reaction mechanisms of insulating SiO_2 have been investigated for decades [1–11]. In these processes, molten $CaCl_2$, which has high solubility of O^{2-} ions, is typically used as an electrolyte. The direct contact of an electric conductor with SiO_2 in a molten salt enables the reduction of SiO_2 to Si by the following solid-state reaction:

$$SiO_2 + 4e^- \rightarrow Si + 2O^{2-} \text{ (in } CaCl_2(l), \text{ at 1123 K)} \quad (1)$$

The electrochemical reduction of SiO_2 starts at the conductor/insulator/electrolyte three-phase interphase [1,3,5]. Due to the high electric conductivity of Si at 1123 K, the reduction proceeds by creating a new three-phase interphase (SiO_2/produced Si/$CaCl_2$). Amorphous Si is first formed by electrochemical reduction and then thermally transformed to crystalline Si [3]. According to the thermodynamic consideration using potential–pO^{2-} diagrams, three solid calcium silicates, $CaSiO_3$, $Ca_3Si_2O_7$, and Ca_2SiO_4, were indicated as possible intermediates depending on the pO^{2-} value [6]. Among them, $CaSiO_3$ was suggested to be most likely one by *ex situ* X-ray photoelectron spectroscopy [6].

In situ synchrotron X-ray diffraction is a useful technique for phase identification. Most previous studies of the electrochemical reduction of oxides in molten salts have employed *ex situ* phase identification methods, after cooling and washing the reduction samples. However, the crystal structures of the samples might change during the cooling process, and the washing treatment might induce chemical reactions as well as the removal of water-soluble species. *In situ* synchrotron X-ray diffraction measurements were previously performed to identify the intermediate compounds in the electrochemical reduction of TiO_2 [15] and $NiTiO_3$ [16] in molten $CaCl_2$, as well as of UO_2 [19] in molten LiCl–KCl. In the case of TiO_2, sub-stoichiometric phases such as $CaTiO_3$ and CaO were reported as intermediate products during the reduction reaction [15]. In the reaction of $NiTiO_3$, CaO was not detected and only $CaTiO_3$ was confirmed as an intermediate oxide product [16]. Moreover, no intermediate products were reported for the electrochemical reduction of UO_2 in molten LiCl–KCl [19]. In the present study, *in situ* synchrotron X-ray diffraction was employed to determine the phase

* Corresponding author.
E-mail address: nohira.toshiyuki.8r@kyoto-u.ac.jp (T. Nohira).
[1] Present address: Global Zero Emission Research Center, The National Institute of Advanced Industrial Science and Technology (AIST), 16-1 Onogawa, Tsukuba 305-8569, Japan.
[2] Present address: Department of Materials Science and Engineering, Graduate School of Engineering, Kyoto University, Yoshida-hommachi, Sakyo-ku, Kyoto 606-8501, Japan.

https://doi.org/10.1016/j.elecom.2020.106740
Received 7 March 2020; Received in revised form 2 May 2020; Accepted 4 May 2020
Available online 05 May 2020

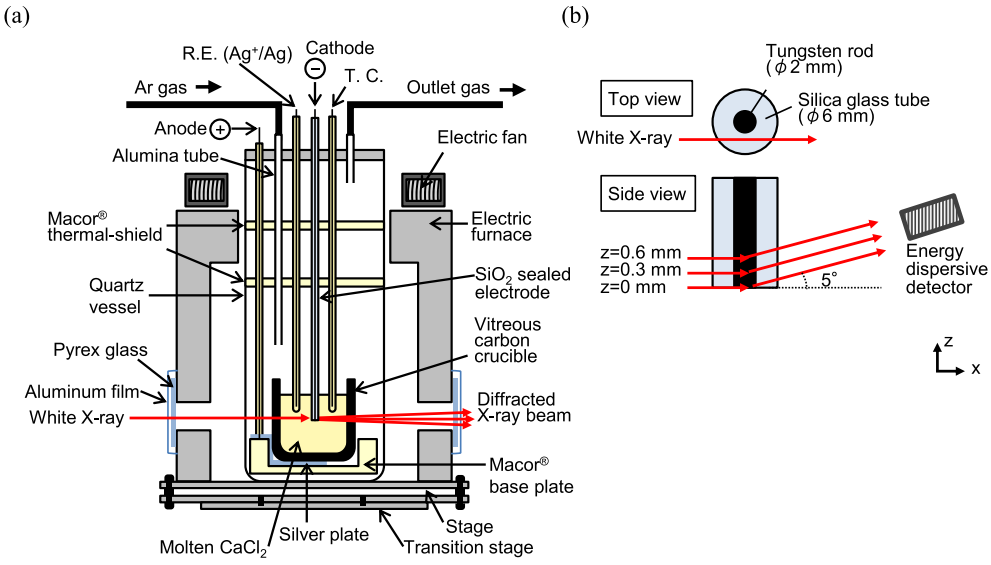

Fig. 1. (a) Schematic illustration of *in situ* experimental apparatus for electrochemical reduction of SiO_2 in molten $CaCl_2$ at 1123 K. (b) Scheme of glass-sealed electrode and beam path.

composition during the electrochemical reduction of SiO_2 in molten $CaCl_2$ and further investigate the corresponding reduction mechanism.

2. Experimental

Fig. 1a shows a schematic illustration of the experimental apparatus. Before the experiment, 25.0 g of $CaCl_2$ (> 95%, Fujifilm Wako Pure Chemical Co., Ltd.) was placed in a vitreous carbon crucible (outer diameter (o.d.) 40 mm, height 40 mm, purity 99%, Tokai Carbon Co., Ltd.) set in an open dry chamber (HRW-60AR, Daikin Co., Ltd.). The crucible containing $CaCl_2$ was successively dried at 453 K for 2 h, at 773 K for 12 h under vacuum, and at 1123 K in dry Ar atmosphere for 6 h. The experiment was carried out at the BL28B2 beamline of SPring-8 in Hyogo, Japan. A vertical electric furnace with four windows was designed to allow white X-rays to penetrate. The electrolysis was conducted inside a quartz glass vessel at 1123 K in a dry Ar atmosphere. To avoid heat damage, the windows were covered with aluminum films. The temperature was controlled by two chromel–alumel thermocouples; one was installed in the vertical furnace and the other was immersed in the molten salt.

Electrochemical measurements and electrolysis were conducted in a three-electrode configuration using an electrochemical measurement system (HZ-7000, Hokuto Denko Corp.). The vitreous carbon crucible and a silver plate (10 mm × 30 mm × 0.1 mm, 99.98%, Nilaco Corp.) were used as counter electrode and current lead, respectively. The reference electrode was an Ag^+/Ag electrode prepared by immersing a silver wire (diameter 1.0 mm, 99%, Nilaco Corp.) in a $CaCl_2$ melt containing 0.5 mol% AgCl (99.5%, Fujifilm Wako Pure Chemical Co., Ltd.) placed in a mullite tube (o.d. 6 mm, inner diameter (i.d.) 4 mm, SiO_2 40%, Al_2O_3 56%, Nikkato Corp.) [6]. The potentials were calibrated by the Ca deposition/dissolution potential measured by an Mo electrode (diameter 1.0 mm, > 99.95%, Nilaco Corp.) [6] before the start of the electrolysis of SiO_2.

Fig. 1b shows a schematic illustration of the glass-sealed electrode and beam paths. The SiO_2 glass-sealed electrode, employed as working electrode, was prepared by inserting a tungsten rod (diameter 2.0 mm, > 99.95%, Nilaco Corp.) into a silica glass (amorphous SiO_2) tube (o.d. 6.0 mm, i.d. 2.0 mm) [12]. Cyclic voltammetry (CV) measurements were performed immediately before the electrolysis (scan rate 100 mV s^{-1}, 1 cycle, potential range 2.0–0.3 V *vs.* Ca^{2+}/Ca). Using the same electrode employed for the CV measurements, the electrolysis was conducted by scanning the potential from the open circuit value to 0.7 V *vs.* Ca^{2+}/Ca at a rate of 0.5 mV s^{-1}, and then keeping the potential at 0.7 V for 150 min. The measurement of the white X-ray diffraction spectrum started at the same time as the potential scan. The size of the incident beam was 50 μm (height) × 200 μm (width) and the take-off angle was set at $2\theta = 5^\circ$. The sizes of the two slits in front of the detector were 50 μm × 3 mm and 50 μm × 8 mm (height × width). The vertical electric furnace was set on the transition stage. The diffracted X-rays were consecutively detected at three different heights: the bottom edge of the electrode ($z = 0$ mm) and two points inside the electrode ($z = 0.3$ and 0.6 mm). The acquisition time for each pattern was 120 s. An energy-dispersive X-ray detector (Ge solid-state detector, GLP-16195/10P4, ORTEC) was employed in the range of 0–200 keV. The number of obtained data points was 4096 (data points for one spectrum) × 30 or 31 (times) × 3 (measured z positions). For each position, a spectrum was obtained with a time resolution of approximately 6 min. The spectra were analyzed in the range of 50–100 keV, which contained around 900 data points.

3. Results and discussion

Fig. 2 shows the potential–time (a) and current–time (b) curves during the electrolysis. During the potential scanning in the negative direction, the cathodic current starts flowing from *ca.* 20 min, corresponding to a potential of 1.3 V. After *ca.* 40 min, the potential remains stable at 0.7 V and the cathodic current around 40 mA lasts until the end of the electrolysis. Such trends agree with the reported starting potential of SiO_2 reduction and with the current values in potentiostatic electrolysis experiments using the same electrode [4,12]. After the experiment, the color of the edge of the SiO_2-sealed electrode changes from colorless to brown, indicating the reduction of SiO_2 to Si.

Fig. 2b–d show the selected energy-dispersive X-ray diffraction (EDXRD) data at $z = 0$, 0.3, and 0.6 mm, respectively. The *d*-spacing values were calculated from the photon energy measured at the detector according to equation (2), derived from Bragg's law with a take-off angle of $2\theta = 5^\circ$:

$$d\,(\text{Å}) \frac{12.40}{2\,E\,\sin\theta\ (\text{keV})} \tag{2}$$

In addition to several peaks for Si [17] and α′-Ca_2SiO_4 [18], the fluorescence peaks of Pb from the beamline instruments appear at 75.03 (Pb $K_{\alpha1}$), 72.76 (Pb $K_{\alpha2}$), 84.68 (Pb $K_{\beta1}$), and 87.48 (Pb $K_{\beta2}$) keV [20,21]. Hereafter, the high temperature α′-Ca_2SiO_4 phase is simply

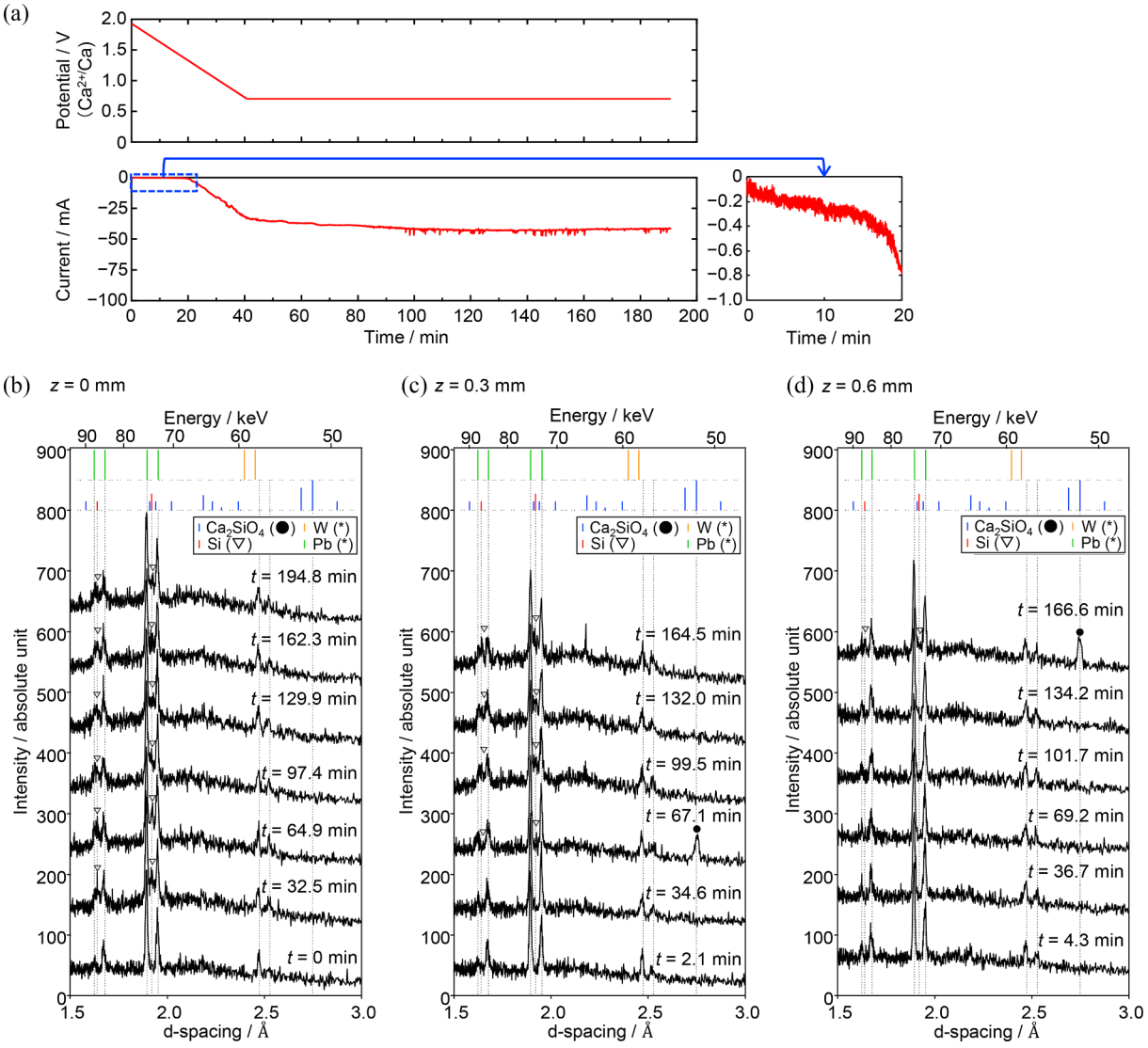

Fig. 2. (a) Potential–time (top) and current–time (bottom) curves during the experiment. (b) Selected raw EDXRD data at different times for (b) $z = 0$ mm, (c) $z = 0.3$ mm, and (d) $z = 0.6$ mm. (*) Peaks from X-ray fluorescence. The shifts of the W fluorescence peaks are due to the energy loss when X-ray is passing through the inside of the electrode.

denoted as Ca_2SiO_4. The peaks at 56.22 and 57.46 keV probably represent shifted W $K_{\alpha1}$ and W $K_{\alpha2}$ fluorescence signals, respectively, and can be attributed to the tungsten rod in the SiO_2-sealed electrode. The shifts of the W fluorescent signals are explained by the energy loss when X-ray is passing through the inside of the electrode consisting of SiO_2, produced Si and Ca_2SiO_4. The measured intensity is shown as raw EDXRD color map data as a function of time in Fig. 3a. A dark red color denotes high-intensity signals. Among the observed signals, the Ca_2SiO_4 (0 2 0) ($E = 51.75$ keV), Si (3 1 1) ($E = 86.78$ keV), and Si (2 2 0) ($E = 74.00$ keV) peaks were used for the evaluation and determination of the reaction products. Among several reported diffraction peaks for Ca_2SiO_4, only the (0 2 0) peak that is the strongest one for Ca_2SiO_4 was observed, indicating that the produced Ca_2SiO_4 had high orientation. Such high orientation might occur when the reaction proceeds in one direction. Incidentally, other possible solid compounds, α-quartz, β-$CaSiO_3$, $Ca_3Si_2O_7$, CaO [21], did not match the peak at $E = 51.75$ keV. The sharp peak at approximately 65 keV at 164.5 min at $z = 0.3$ mm seems to be a background noise taking the width of the peak into account.

Fig. 3b shows the intensity–time curves of the Ca_2SiO_4 (0 2 0), Si (3 3 1), and Si (2 2 0) peaks at each z position indicated in Fig. 3a. At $z = 0$ mm, the formation of Si is observed after 25 min, which matches the time when the reduction current starts flowing at 1.3 V in Fig. 2a. On the other hand, Ca_2SiO_4 is not detected at $z = 0$ mm during the electrolysis. At $z = 0.3$ mm, the Si (3 3 1) and Si (2 2 0) signals increase after 60 min. At the same time, the Ca_2SiO_4 (0 2 0) signal also increases and then drops within 25 min. Similar trends, *i.e*, simultaneous signal increases for Si (3 3 1), Si (2 2 0), and Ca_2SiO_4 (0 2 0), are observed after 150 min at $z = 0.6$ mm. A different feature with respect to the trend observed for $z = 0.3$ mm is that the Si (3 3 1) and Si (2 2 0) signals increase more gradually at $z = 0.6$ mm, indicating that the reduction rate slows down going from the edge to the interior of the electrode. The 1-h reduction rate of SiO_2 observed in the present study (*ca.* 300 μm for 1 h) is consistent with that reported in a previous study (approximately 200 μm at 1.00 V and 400 μm at 0.70 V in the initial 1 h) [4].

Herein, the edge ($z = 0$ mm) and interior ($z = 0.3$ and 0.6 mm) of the electrode exhibit different behaviors in terms of formation of Ca_2SiO_4 and reduction rate of SiO_2. These differences can be explained by the different diffusivity of O^{2-} ions in molten $CaCl_2$ permeated into the electrode. Due to their low diffusivity inside the electrode, the electrochemically produced O^{2-} ions tend to accumulate, which results

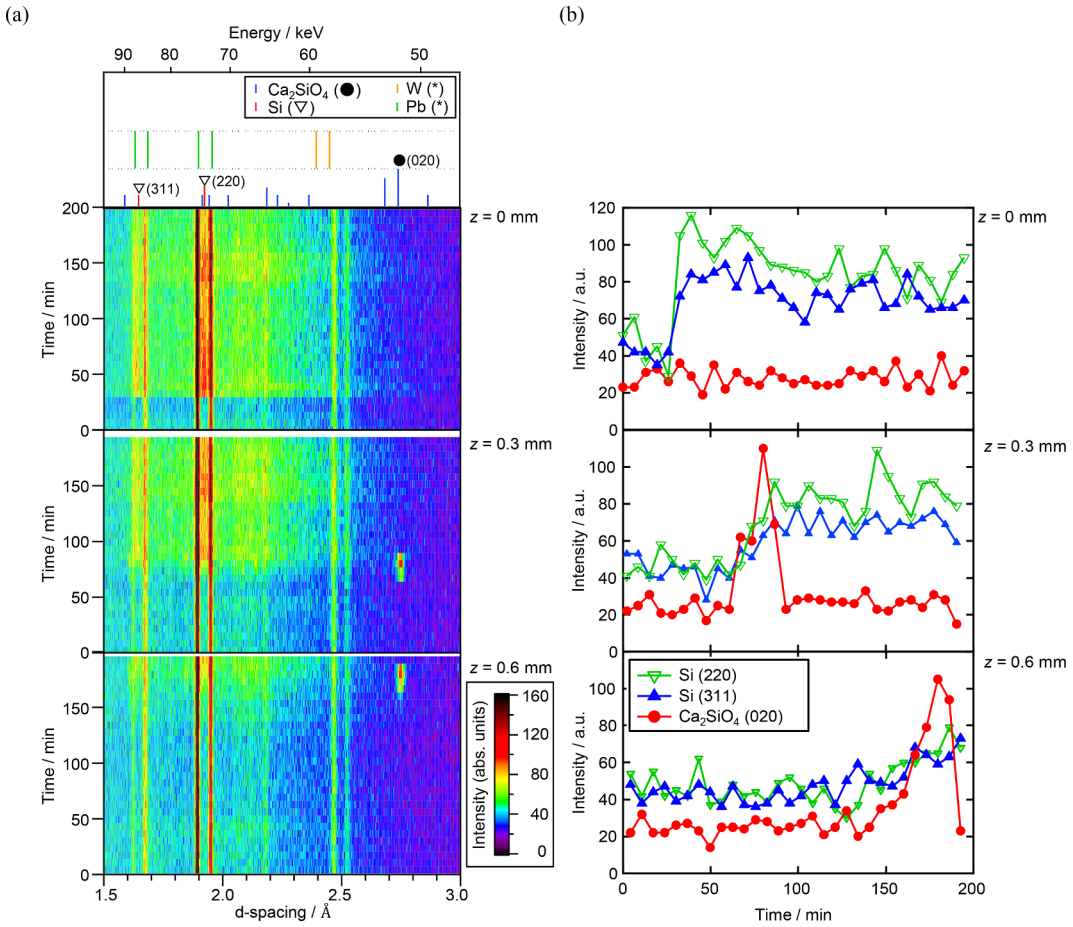

Fig. 3. (a) Color map from raw EDXRD data as a function of time for $z = 0$, 0.3, and 0.6 mm. (*) Peaks from X-ray fluorescence (note: the reason for the shift of the W fluorescence peak is unclear). (b) Intensity–time curves for Ca_2SiO_4 (0 2 0) ($E = 51.75$ keV), Si (3 3 1) ($E = 86.78$ keV), and Si (2 2 0) ($E = 74.00$ keV) signals at each z position.

in slow electrochemical reduction *via* formation of the Ca_2SiO_4 intermediate. On the other hand, since O^{2-} ions are easily removed from the edge of the electrode, fast electrochemical reduction without formation of Ca_2SiO_4 occurs in this region. The potential–pO^{2-} diagram of the Ca–Si–O system [6,13] confirms the stability of calcium silicates in low pO^{2-} (*i.e.*, high O^{2-} ion concentration) regions.

The present study reveals both similar and different trends compared with previous *in situ* synchrotron X-ray diffraction studies of the electrochemical reduction of TiO_2 [15] and $NiTiO_3$ pellets [16]. It should be noted that the dense SiO_2 electrode was used in the present experiment, and that TiO_2 and $NiTiO_3$ porous pellets were used in the previous researches. The similar trend is represented by the lower reduction rate inside the electrode, which applies to all three investigated cases (SiO_2, TiO_2, and $NiTiO_3$). The different behavior concerns the lifetime of the intermediate phases. The lifetime of the $CaTiO_3$ intermediate was more than 4 h for TiO_2 and $NiTiO_3$ even at the edge of the electrode, while in the case of SiO_2, the Ca_2SiO_4 lifetime at the edge of the electrode was only around 25 min. The different lifetime is probably due to the different stability of the intermediates. Even though porous pellets were used in the previous studies of TiO_2 and $NiTiO_3$, which is advantageous for fast diffusion of O^{2-} ions, the lifetime was much longer than that of the present system, involving dense SiO_2, which reflects the high stability of $CaTiO_3$. Moreover, the different electrode configurations (two- and three-electrode systems were used in the previous studies and the present one, respectively) might influence the electrochemical reduction behavior. Clearly, the three-electrode system is preferable for the precise control of the working electrode potential. Since much faster reduction rate was reported for SiO_2 powders piled on a current collector (approximately 3 mm at 0.80 V and 4 mm at 0.60 V in the initial 1 h) [11], *in-situ* X-ray diffraction study is also needed for SiO_2 porous pellets or powders.

4. Conclusions

The electrochemical reduction of SiO_2 to Si in molten $CaCl_2$ at 1123 K was investigated by *in situ* synchrotron X-ray diffraction using a SiO_2 sealed electrode. The Ca_2SiO_4 phase was detected inside the electrode as an intermediate product formed during the electrochemical reduction of SiO_2 to Si, whereas the same phase was not detected at the edge of the electrode. The difference in Ca_2SiO_4 formation behavior can be explained by the occurrence of different O^{2-} ion concentrations at different locations. As the reduction proceeded, the Ca_2SiO_4 phase disappeared in 25 min. Finally, the reduction rates of SiO_2 were observed to decrease from the edge toward the interior of the electrode.

CRediT authorship contribution statement

Yumi Katasho: Conceptualization, Validation, Formal analysis, Investigation, Resources, Data curation, Writing - original draft, Writing - review & editing, Visualization, Funding acquisition. **Yutaro Norikawa:** Validation, Investigation, Resources, Writing - review & editing. **Takayuki Yamamoto:** Validation, Investigation, Resources, Writing - review & editing. **Kouji Yasuda:** Validation, Investigation, Resources, Writing - original draft, Writing - review & editing. **Toshiyuki Nohira:** Conceptualization, Validation, Investigation, Resources, Writing - original draft, Writing - review & editing, Supervision, Project administration, Funding acquisition.

Declaration of Competing Interest

The authors declare that they have no known competing financial interests or personal relationships that could have appeared to influence the work reported in this paper.

Acknowledgments

This work was supported by JSPS KAKENHI Grant Number 17J08901 and 16H02410. The synchrotron radiation experiments were performed at the BL28B2 of SPring-8 with the approval of the Japan Synchrotron Radiation Research Institute (JASRI) (Proposal No. 2017B1682). The authors thank Dr. Kentaro Kajiwara at JASRI for his assistance on operating the beamline.

References

[1] T. Nohira, K. Yasuda, Y. Ito, Pinpoint and bulk electrochemical reduction of insulating silicon dioxide to silicon, Nat. Mater. 2 (2003) 397–401, https://doi.org/10.1038/nmat900.

[2] X. Jin, P. Gao, D. Wang, X. Hu, G.Z. Chen, Electrochemical preparation of silicon and its alloys from solid oxides in molten calcium chloride, Angew. Chem. 43 (2004) 733–736, https://doi.org/10.1002/anie.200352786.

[3] K. Yasuda, T. Nohira, K. Amezawa, Y.H. Ogata, Y. Ito, Mechanism of direct electrolytic reduction of solid SiO_2 to Si in molten $CaCl_2$, J. Electrochem. Soc. 152 (2005) D69–D74, https://doi.org/10.1149/1.1864453.

[4] K. Yasuda, T. Nohira, Y. Ito, Effect of electrolysis potential on reduction of solid silicon dioxide in molten $CaCl_2$, J. Phys. Chem. Solids. 66 (2005) 443–447, https://doi.org/10.1016/j.jpcs.2004.06.037.

[5] W. Xiao, X. Jin, Y. Deng, D. Wang, X. Hu, G.Z. Chen, Electrochemically driven three-phase interlines into insulator compounds: Electroreduction of solid SiO_2 in molten $CaCl_2$, ChemPhysChem. 7 (2006) 1750–1758, https://doi.org/10.1002/cphc.200600149.

[6] K. Yasuda, T. Nohira, R. Hagiwara, Y.H. Ogata, Diagrammatic representation of direct electrolytic reduction of SiO_2 in molten $CaCl_2$, J. Electrochem. Soc. 154 (2007) E95–E101, https://doi.org/10.1149/1.2736641.

[7] S.K. Cho, F.R.F. Fan, A.J. Bard, Electrodeposition of crystalline and photoactive silicon directly from silicon dioxide nanoparticles in molten $CaCl_2$, Angew. Chem. 51 (2012) 12740–12744, https://doi.org/10.1002/anie.201206789.

[8] Y. Deng, D. Wang, W. Xiao, X. Jin, X. Hu, G.Z. Chen, Electrochemistry at conductor/insulator/electrolyte three-phase interlines: A thin layer model, J. Phys. Chem. B. 109 (2005) 14043–14051, https://doi.org/10.1021/jp044604r.

[9] E. Juzeliunas, D.J. Fray, Silicon electrochemistry in molten salts, Chem. Rev. 120 (3) (2020) 1690–1709, https://doi.org/10.1021/acs.chemrev.9b00428.

[10] J. Ge, X. Zou, S. Almassi, Ji Li, B.P. Chaplin, A.J. Bard, Electrochemical production of Si without generation of CO_2 based on the use of a dimensionally stable anode in molten $CaCl_2$, Angew. Chem. Int. Ed. 58 (2019) 16223–16228, https://doi.org/10.1002/anie.201905991.

[11] X. Yang, K. Yasuda, T. Nohira, R. Hagiwara, T. Homma, Cathodic potential dependence of electrochemical reduction of SiO_2 granules in molten $CaCl_2$, Metall. Mater. Trans. E 3 (2016) 145–155, https://doi.org/10.1007/s40553-016-0081-1.

[12] Y. Katasho, X. Yang, K. Yasuda, T. Nohira, Electrochemical reduction behavior of borosilicate glass in molten $CaCl_2$, J. Electrochem. Soc. 163 (2016) D622–D627, https://doi.org/10.1149/2.0971610jes.

[13] Y. Katasho, K. Yasuda, T. Nohira, Behaviors of Si, B, Al, and Na during electrochemical reduction of borosilicate glass in molten $CaCl_2$, J. Electrochem. Soc. 164 (2017) D478–D485, https://doi.org/10.1149/2.1201707jes.

[14] Y. Katasho, K. Yasuda, T. Nohira, Electrochemical reduction behavior of simplified simulants of vitrified radioactive waste in molten $CaCl_2$, J. Nucl. Mater. 503 (2018) 290–303, https://doi.org/10.1016/j.jnucmat.2018.03.006.

[15] R. Bhagat, D. Dye, S.L. Raghunathan, R.J. Talling, D. Inman, B.K. Jackson, K.K. Rao, R.J. Dashwood, In situ synchrotron diffraction of the electrochemical reduction pathway of TiO_2, Acta Mater. 58 (2010) 5057–5062, https://doi.org/10.1016/j.actamat.2010.05.041.

[16] B.K. Jackson, D. Dye, D. Inman, R. Bhagat, R.J. Talling, S.L. Raghunathan, M. Jackson, R.J. Dashwood, Characterization of the FFC Cambridge process for NiTi production using in situ X-ray synchrotron diffraction, J. Electrochem. Soc. 157 (2010) E57–E63, https://doi.org/10.1149/1.3299369.

[17] PDF-00-027-1402; National Bureau of Standards (United States), National Bureau of Standards Monograph, 2513 (1976) 35.

[18] PDF-20-0237; G. Yamaguchi, Y. Ono, S. Kawamura, Y. Soda, Synthesis of the modifications of Ca2SiO4 and the determination of their powder X-ray diffraction patterns, J. Ceram. Assoc. Jpn., 71 (1963) 63–68. doi.org/10.2109/jcersj1950.71.806_63.

[19] L.D. Brown, R. Abdulaziz, R. Jervis, V.J. Bharath, R.C. Attwood, C. Reinhard, L.D. Connor, S.J.R. Simons, D. Inman, D.J.L. Brett, P.R. Shearing, Following the electroreduction of uranium dioxide to uranium in LiCl–KCl eutectic in situ using synchrotron radiation, J. Nucl. Mater. 464 (2015) 256–262, https://doi.org/10.1016/j.jnucmat.2015.04.037.

[20] H. Yamada, H. Saisho, T. Hirai, J. Hirano, X-ray fluorescence analysis of heavy elements with a portable synchrotron, Spectrochim, Acta - Part B At. Spectrosc. 59 (2004) 1323–1328, https://doi.org/10.1016/j.sab.2004.04.013.

[21] PDF-33-1161 (α-quartz), PDF-42-0550 (β-$CaSiO_3$), PDF-29-0370 ($Ca_3Si_2O_7$), PDF-37-1497 (CaO).